Propagation Characteristics of a Heaviside Absorbing Layer for TLM

Ian G. Gosling, *Senior Member, IEEE,* and Pingyu Qu

***Abstract*—The perfectly matched layer for use with the finite-difference time-domain method is adapted to our transmission-line matrix simulation as what we call a heaviside absorbing layer (HAL). It is shown that the reflection coefficient for the wave incident on a HAL is less than that of the wave incident on a matched-load termination at all angles of incidence. Furthermore, the dispersion relation of a transmission-line matrix mesh of a symmetrical condensed node with both electric and magnetic loss stubs is derived. It provides guidance on how to choose the losses of HAL and other simulation parameters properly.**

***Index Terms*—TLM, absorbing boundary.**

I. Introduction

THE TRANSMISSION-LINE matrix (TLM) method has been successfully applied to solve electromagnetic wave propagation, scattering, and diffraction problems in the time domain. In order to truncate the computation region and avoid unwanted nonphysical reflection, an absorbing boundary is needed. Several absorbing boundary conditions have been proposed [1]–[3]. For the TLM mesh of symmetrical condensed nodes (SCN) the absorbing boundary is usually realized by terminating the link lines at the edge of the mesh in their own characteristic impedance, so that the incident waves are absorbed completely. However, it is shown in [4] that this absorbing boundary only works for the wave at 0° angle of incidence to the boundary. For other angles of incidence, large unwanted reflections still exist. Some improvements have been made in [4] and [5].

Recently, the so-called perfectly matched layer (PML) absorbing boundary condition was mentioned [6] for use with the finite-difference time-domain (FDTD) method. One of the important characteristics of PML is that it possesses both electric loss σ_e and magnetic loss σ_m restricted by the condition

$$\sigma_m = \frac{\mu_0}{\epsilon_0}\sigma_e. \tag{1}$$

In [6] it was shown that for a certain frequency range, the reflection coefficient Γ of a PML of 20-cells thick can be as low as -60 dB.

A so-called heaviside absorbing layer (HAL) is presented in this paper for use with the TLM method. The HAL consists of a physically unrealizable medium with $\mu = \mu_0$, $\epsilon = \epsilon_0$ and both σ_e and σ_m, satisfying (1). In Section II, the characteristic parameters of a HAL are presented. Then, the reflection coefficient Γ for the wave incident in a HAL is calculated using Maxwell's equations and boundary conditions. In Section IV, the dispersion properties of a TLM mesh of SCN with loss stubs are analyzed. The method is applied to a HAL. Finally, the analytical results are verified by computer simulation using our lossy TLM code.

Manuscript received March 5, 1996; revised October 18, 1996.

The authors are with the School of Electrical and Electronic Engineering, Nanyang Technologial University, 639798 Singapore.

Publisher Item Identifier S 0018-9480(97)00834-X.

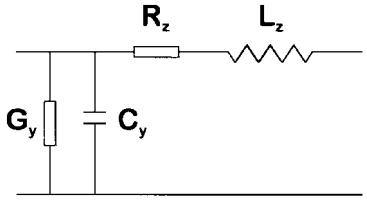

Fig. 1. Equivalent circuit for the wave traveling along a lossy TLM mesh axis.

II. Characteristics of a HAL

In a source-free, infinite HAL region, two of Maxwell's equations are

$$\nabla \times \vec{E} = -j\omega\mu_0\vec{H} - \sigma_m\vec{H} \tag{2}$$

$$\nabla \times \vec{H} = j\omega\epsilon_0\vec{E} + \sigma_e\vec{E}. \tag{3}$$

Thus, follows the Helmholtz equation:

$$\nabla^2\vec{E} - \frac{\mu_0}{\epsilon_0}(j\omega\epsilon_0 + \sigma_e)^2\vec{E} = 0. \tag{4}$$

For a TEM plane wave traveling in a HAL, we have

$$\gamma^2 = \frac{\mu_0}{\epsilon_0}(j\omega\epsilon_0 + \sigma_e)^2 \tag{5}$$

$$Z_{\mathrm{HAL}} = \frac{j\omega\mu_0 + \sigma_m}{\gamma} = Z_0 \tag{6}$$

where γ and Z_{HAL} are the propagation constant and intrinsic impedance for the TEM wave traveling in an infinite HAL region, respectively, and Z_0 is the intrinsic impedance of free space. From (5) and (6) it can be seen that the intrinsic impedance and phase constant in the HAL are the same as those of free space.

To model the lossy medium with both electric loss σ_e and magnetic loss σ_m, an SCN formulation was developed with six more stubs added to Johns' original node, three to model electric loss and three to model magnetic loss. For the wave traveling along the mesh axis, e.g., the x direction, over one TLM SCN cell, the equivalent circuit is drawn in Fig. 1, where C_y, L_z are the total capacitance and inductance and G_y, R_z are

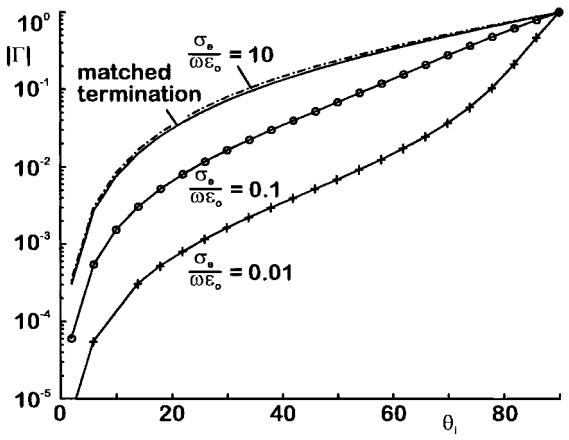

Fig. 2. Variation of Γ with $\sigma_e/\omega\epsilon_0$.

admittance and resistance per unit length representing electric loss and magnetic loss, respectively.

According to the transmission-line theory in [7]:

$$Z_{\mathrm{HAL}} = \sqrt{\frac{R_s + j\omega L_z}{G_y + j\omega C_y}} \tag{7}$$

$$\gamma = \frac{\sqrt{(R_z + j\omega L_z)(G_y + j\omega C_y)}}{u} \tag{8}$$

where u is the cell dimension along the x direction. By using the equivalence in [8] and [9], and equal mesh spacing in all three dimensions, a heaviside transmission line having $Z_{\mathrm{HAL}} = Z_0$ is obtained.

III. HAL Absorbing Condition

The absorbing properties of the HAL are studied by calculating the reflection coefficient Γ of a plane-wave incident from free space into a semi-infinite HAL medium.

Consider a wave incident at an angle θ_i from free space on to a semi-infinite HAL medium. From (2) and (3), the equivalent complex permittivity and permeability of the HAL medium are

$$\mu_2 = \mu_0 - j\frac{\sigma_m}{\omega}, \qquad \epsilon_2 = \epsilon_0 - j\frac{\sigma_e}{\omega}. \tag{9}$$

Hence, the refractive index of the HAL is given by

$$n_2 = \sqrt{\frac{\epsilon_2\mu_2}{\epsilon_0\mu_0}}. \tag{10}$$

From [10] and [11], the reflection coefficient in the case of parallel polarization is

$$\Gamma^{\parallel} = \frac{\cos\theta_i - \cos\theta_t}{\cos\theta_i + \cos\theta_t} \tag{11}$$

and in the case of perpendicular polarization is

$$\Gamma^{\perp} = \frac{\cos\theta_t - \cos\theta_i}{\cos\theta_t + \cos\theta_i}. \tag{12}$$

The complex angle of transmission θ_t is found from Snell's law:

$$1 \times \sin\theta_i = n_2 \sin\theta_t \tag{13}$$

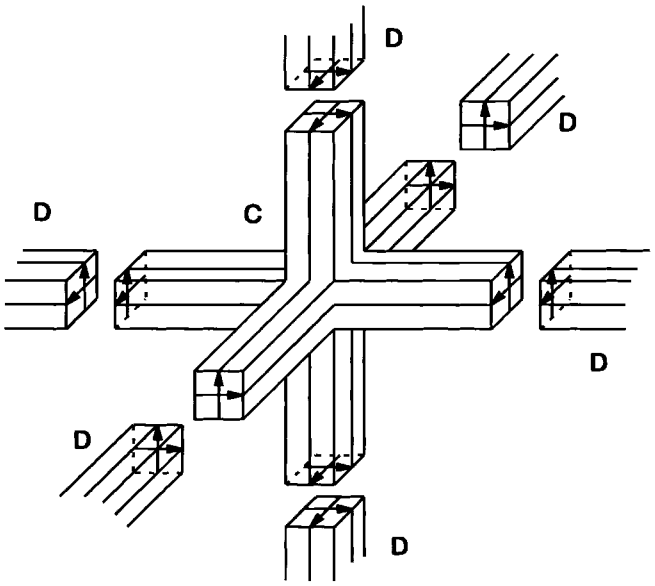

Fig. 3. Two nodes used in dispersion analysis.

which, from above, can be rewritten as

$$\cos\theta_t = \sqrt{1 - \frac{\sin^2\theta_i}{\left(1 - j\frac{\sigma_e}{\omega\epsilon_o}\right)^2}}. \tag{14}$$

The variation of Γ with loss tangent $\sigma_e/\omega\mathbf{e}_0$ is shown in Fig. 2. As a comparison, the reflection coefficient Γ_0 of a plane-wave incident on a matched-load terminated TLM mesh is also presented. It can be seen that Γ is about 30 dB less than Γ_0 for angles of incidence between 0° and 40° when $\sigma_e/\omega\epsilon_0 = 0.01$. The higher the frequency and the smaller the losses, the smaller Γ will be.

IV. Dispersion Properties of HAL

A. Dispersion Relation of TLM SCN with Loss Stubs

It is reasonable to assume that the dispersion properties of SCN without loss stubs will be changed when extra loss stubs are introduced. Thus, in order to further verify the reduction of reflection using our lossy TLM code, it is necessary to analyze the dispersion properties of the HAL so that the simulation parameters can be chosen properly.

The dispersion analysis of general SCN with both electric and magnetic loss stubs is conducted following the method in [12]. Two nodes are considered in the dispersion analysis. One is the conventional symmetrical condensed node, denoted as node C. The other is a conglomerate node D composed of six adjacent nodes surrounding C (Fig. 3). The formulation in [12] is based on the separation of V's at node C in open or short stubs and the contributions of 12 link lines. However, in our case there are 24 V's in the reflected V vector, i.e., 12 for link lines, six for open or short stubs, and another six for electric or magnetic loss stubs. The dimension of the incident V vector remains at 18×1 since there are no incident waves from the terminated ends of the loss stubs. Thus, the useful

scattering matrix is 24 × 18 and the submatrices are different. At an arbitrary moment $t_n = t_0 + n\Delta t$:

$$\begin{bmatrix} v_c^r \\ v_{c,\,s}^r \\ v_{c,\,l}^r \end{bmatrix}_{t_n} = \begin{bmatrix} S & G \\ E & H \\ M & N \end{bmatrix} \begin{bmatrix} v_c^i \\ v_{c,\,s}^i \end{bmatrix}_{t_n} \tag{15}$$

where superscripts i and r represent incident and reflected V, respectively, subscripts $c,\ s$ and $c,\ l$ stand for dielectric stubs and loss stubs, respectively, at node C. The original scattering matrix has been divided into six submatrices: $S(12 \times 12)$; $G(12 \times 6)$; $E(6 \times 12)$; $H(6 \times 6)$; $M(6 \times 12)$; and $N(6 \times 6)$.

After some manipulation similar to [12], the relation between incident V's and reflected V's in the link lines is found to be

$$[v_c^r]_{t_n} = [S + GQT_sAE][v_c^i]_{t_n} \tag{16}$$

where Q is a 6×6 diagonal matrix with $Q_{11} = Q_{22} = Q_{33} = 1$ and $Q_{44} = Q_{55} = Q_{66} = -1$, $T_s = e^{-jk_0\frac{\Delta l}{2}} I_0$, I_0 being the 6×6 identity matrix and A is the 6×6 matrix:

$$[A] = \sum_{n=0}^{\infty} [HQT_s]^n. \tag{17}$$

Besides (16), two more important relations are used in our analysis:

1) propagation between adjacent nodes:

$$[v_c^i]_{t_n} = T[v_d^r]_{t_n} \tag{18}$$

where T is a 12×12 diagonal matrix whose nonzero elements are $T_{ii} = e^{-jk_0\frac{\Delta l}{2}}$ for $i = 1, \cdots, 12$;

2) Floquet's theorem. For a TLM SCN mesh with loss stubs, γ will no longer be a pure imaginary number but rather a complex one, accounting for the damping effect of losses:

$$[v_c^r]_{t_n} = P[v_d^r]_{t_n} \tag{19}$$

where P is 12×12 matrix whose nonzero elements are

$$\begin{aligned} P_{1,\,12} &= P_{5,\,7} = e^{\gamma_y \Delta l} \\ P_{2,\,9} &= P_{4,\,8} = e^{\gamma_z \Delta l} \\ P_{3,\,11} &= P_{6,\,10} = e^{\gamma_x \Delta l} \\ P_{7,\,5} &= P_{12,\,1} = e^{\gamma_y \Delta l} \\ P_{8,\,4} &= P_{9,\,2} = e^{\gamma_z \Delta l} \\ P_{10,\,6} &= P_{11,\,3} = e^{\gamma_x \Delta l} \end{aligned} \tag{20}$$

where γ_x, γ_y, and γ_z are the components of the plane-wave propagation constants in a lossy TLM mesh.

A dispersion relation similar to that in [12] is derived for a lossy SCN with uniform mesh spacing by combining (16), (18), and (19):

$$\det\left[I - TPS - TPGQT_sAE\right] = 0. \tag{21}$$

Equation (21) is solved using algebraic solver software for γ pointing along three typical directions $(1, 0, 0)$, $(1, 1, 0)$ and $(1, 1, 1)$. In the ideal dispersionless case, all the frequency components of a plane wave propagating in the HAL should have phase velocity $v_p = c$, the speed of light, and the same attenuation constant $\sigma_e Z_0$. Thus, the dispersion properties of HAL can be represented in terms of the frequency-dependent phase velocities v_p normalized by c and the frequency-dependent attenuation per-space step $\alpha\Delta l$ normalized by $R = \sigma_e Z_0 \Delta l$.

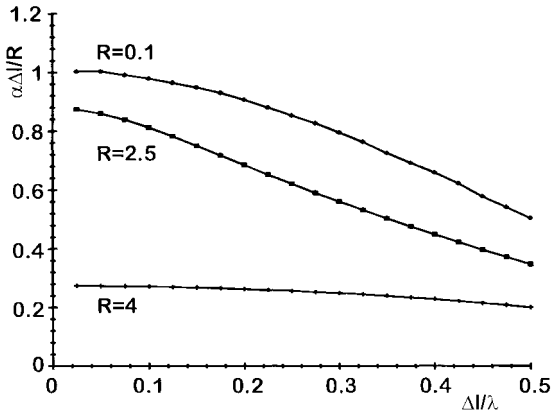

Fig. 4. Variation of $\alpha\Delta l/R$ with $\Delta l/\lambda$ for several cases of R along $(1, 0, 0)$.

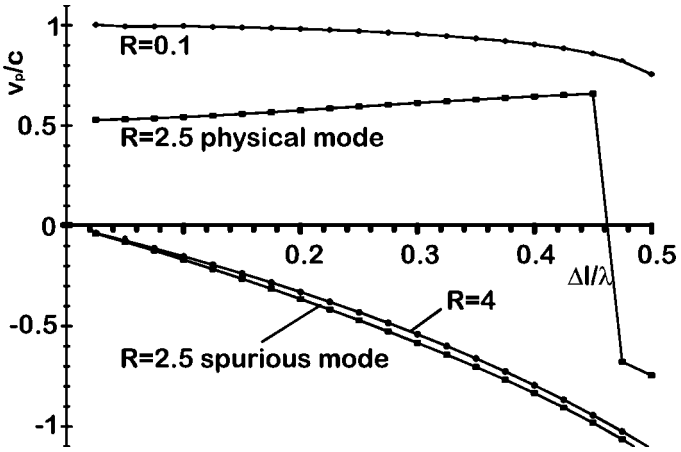

Fig. 5. Variation of v_p/c with $\Delta l/\lambda$ for several cases of R along $(1, 0, 0)$.

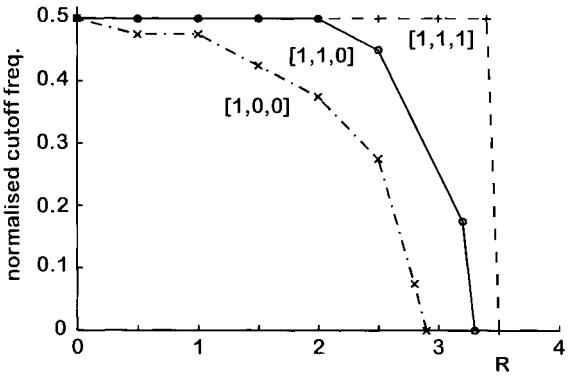

Fig. 6. Cutoff frequency variation with R.

B. Dispersion Along Direction (1, 0, 0)

The dispersion properties along $(1, 0, 0)$ are derived by assuming any two of the three propagation constants along

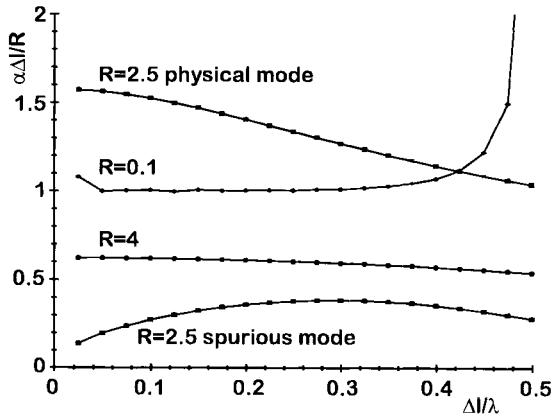

Fig. 7. Variation of $\alpha\Delta l/R$ with $\Delta l/\lambda$ for several cases of R along $(1,1,0)$.

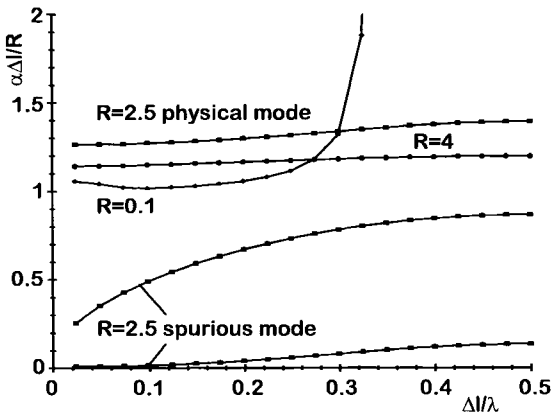

Fig. 9. Variation of $\alpha\Delta l/R$ with $\Delta l/\lambda$ for several cases of R along $(1,1,1)$.

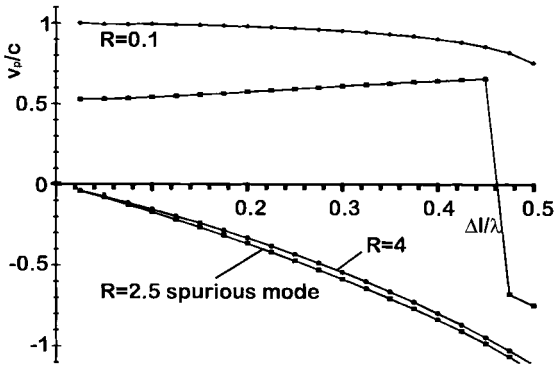

Fig. 8. Variation of v_p/c with $\Delta l/\lambda$ for several cases of R along $(1,1,0)$.

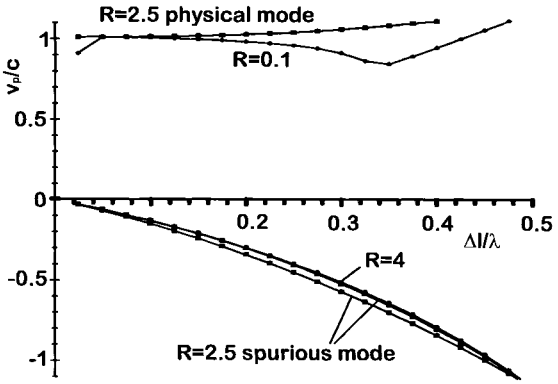

Fig. 10. Variation of v_p/c with $\Delta l/\lambda$ for several cases of R along $(1,1,1)$.

the axes in (21) to be zero. The results are shown in Figs. 4 and 5 for several cases of R. Several important conclusions can be reached.

- The dispersion properties of the HAL are dependent on R rather than σ_e alone.
- For a HAL with small R, apart from the attenuation introduced by the loss, the dispersion properties of the mesh are similar to those without loss stubs, i.e., $v_p/c \approx 1$ and no cutoff frequency due to mesh spacing.
- As R increases, v_p decreases. Above a cutoff frequency, the wave becomes a nonphysical backward wave. (This is not the same cutoff frequency as that due to the mesh spacing.) Fig. 6 shows the variation of this cutoff frequency with R. It can be seen that it decreases with R, becoming zero when $R = 2.8$.

C. Dispersion Along Direction (1,1,0)

In this case, one of the propagation constants is assumed to be zero and the two others are assumed to be equal in (21). The variation of $\alpha\Delta l/R$ and v_p/c with frequency is shown in Figs. 7 and 8 for several cases of R. The behavior is similar to that of the $(1,0,0)$ direction except for the following.

- The cutoff frequency, where the physical wave solution becomes a backward wave, approaches zero at $R = 3.3$. The change of cutoff frequency with R is also shown in Fig. 6.
- There exists two solutions to (21). One is the physical mode and the other is the spurious mode. In Figs. 7 and 8, both modes are shown for the case when $R = 2.5$.

D. Dispersion Along Direction (1,1,1)

In this case, all of the three propagation constants are assumed to be equal in (21). The variation of $\alpha\Delta l/R$ and v_p/c with frequency is shown in Figs. 9 and 10 for several cases of R. The following comments can be made.

- The cutoff frequency approaches zero at $R = 3.5$. Unlike the $(1,0,0)$ and $(1,1,0)$ directions, in which the cutoff frequency changes gradually with R, the cutoff frequency in $(1,1,1)$ switches from 0.5 to 0 abruptly when R increases from 3.4 to 3.5, as shown in Fig. 6.
- There exist three solutions to (21). One of them is the physical mode and the other two solutions are the spurious modes. In Figs. 9 and 10, both modes are shown for the case when $R = 2.5$.

V. Simulation Results

A. TLM Simulation of Wave Dispersion

In order to verify the dispersion analysis presented in Section IV, the propagation properties of a plane wave traveling in a HAL along the three directions were examined by our TLM simulation. For propagation along the $(1,0,0)$ direction,

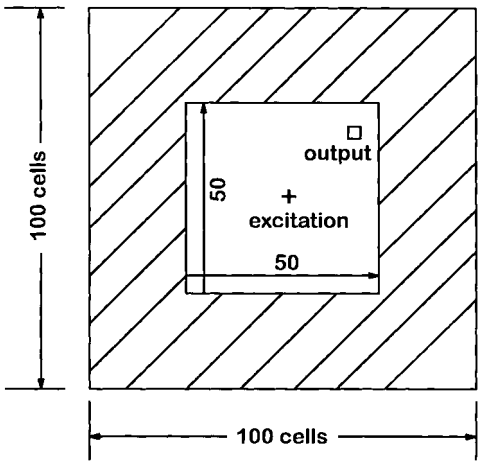

Fig. 11. Line source radiation into free space with and without HAL termination.

TABLE I
COMPARISON BETWEEN DISPERSION ANALYSIS AND SIMULATION IN DIRECTION $(1,0,0)$ WHEN $R = 2.5$

$\Delta l/\lambda$	v_p/c		$\exp(-\alpha\Delta l)$	
	theoretical	simulation	theoretical	simulation
0.1	0.2122	0.2121	0.1312	0.1312
0.2	0.4191	0.4191	0.1803	0.1804
0.3	-0.6097	-0.6100	0.2460	0.2462
0.4	-0.8938	-0.8939	0.3247	0.3241
0.5	-1.2675	-1.2685	0.4186	0.4190

a plane wave traveling in a parallel plate waveguide was simulated. For the $(1,1,0)$ direction, the simulation was performed by exciting a plane wave with proper field components along the diagonal line of a two–dimensional (2-D) square region. For the $(1,1,1)$ direction, the simulation was done in a $60 \times 60 \times 60$ cube in which a plane wave was stimulated properly along the diagonal plane.

Both attenuation and v_p/c that were measured in the simulation fit very well with the above dispersion analysis for small or large R. The nonphysical mode predicted by the dispersion analysis was also verified. For $(1,1,0)$ and $(1,1,1)$ directions, only the physical mode was detected in the simulation output. Table I lists both the simulation and the dispersion analysis for $R = 2.5$ along the $(1,0,0)$ direction at several normalized frequency points.

B. Application of HAL

The improvement in boundary absorption afforded by the HAL was verified by the TLM simulation of a line source radiating into free space in the cases with and without the mesh terminated by HAL cells. From the dispersion analysis we know that R should not be set too large, in order to prevent propagation of nonphysical modes. On the other hand, σ_e and the thickness of the HAL cells should not be too small, so that the wave can be attenuated effectively in the HAL and reflection from the final boundary at the edge of the TLM mesh will not be significant. Bearing this in mind, σ_e was chosen as 0.015.

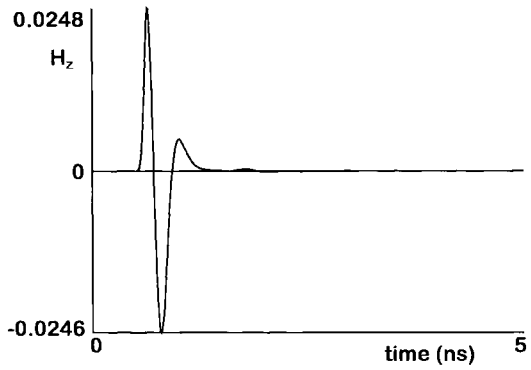

Fig. 12. Output field in the time domain with HAL termination.

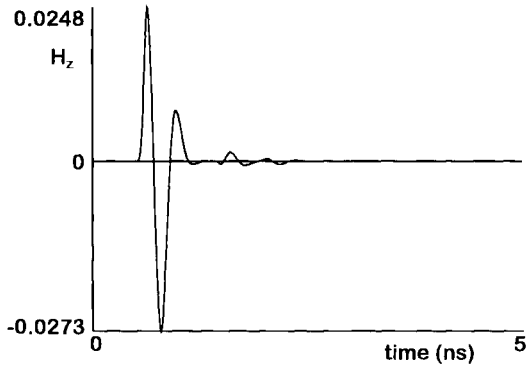

Fig. 13. Output field in the time domain without HAL termination.

The excitation and output points are the same for both sample cases, as shown in Fig. 11. A band-limited Gaussian pulse is used as the excitation field. The waveform of the field H_z at the output point in the time domain for the two cases is shown in Figs. 12 and 13, respectively. It can be clearly seen that the reflection was improved when HAL was used.

VI. CONCLUSION

In this paper we have presented a new absorbing boundary, HAL, for the use with the TLM method. The theoretical analysis shows that the reflection coefficient for the wave incident on a HAL is about 30 dB less than that of the wave incident on a matched-load termination at incident angles between 0° and 40° when $\sigma_e/\omega\epsilon_o = 0.01$. The dispersion relation of a SCN TLM mesh with both electric and magnetic loss stubs has been derived. The method is applied to analyze the dispersion in the HAL and the results are compared with the TLM simulation. It has been shown that there is a cutoff frequency which decreases when R increases, where the physical propagation mode changes into a backward wave. Beyond a certain limit of R, a nonphysical propagation mode will dominate. This suggests that we should not exceed a certain value of frequency or of R in the TLM simulation.

REFERENCES

[1] U. Muller, A. Beyer, and M. Rittweger, "Simulations with the 3D TLM SCN using FD-TD absorbing boundary conditions," in *IEEE MTT-S Dig.*, pp. 377–380, 1992.

[2] J. A. Morente, J. A. Porti, and M. Khalladi, "Absorbing boundary conditions for the TLM method," *IEEE Trans. Microwave Theory Tech.*, vol. 40, pp. 2095–2099, 1992.
[3] N. R. S. Simons and E. Bridges, "Application of the TLM method to two-dimensional scattering problems," *Int. J. Numer. Modelling*, vol. 5, pp. 93–110, 1992.
[4] ——, "Method for modelling free space boundaries in TLM situations," *Electron. Lett.*, vol. 26, pp. 453–455, 1990.
[5] I. G. Gosling, "Reduction of edge reflections in the TLM model," *IEEE Trans. Microwave Theory Tech.*, vol. 41, pp. 1057–1064, 1993.
[6] E. A. Navarro, C. Wu, P. Y. Chung, and J. Litva, "Application of PML superabsorbing boundary condition to non-orthogonal FDTD method," *Electron. Lett.*, vol. 30, pp. 1654–1656, 1994.
[7] R. E. Collin, *Foundations for Microwave Engineering.* New York: McGraw-Hill, 1966.
[8] P. B. Johns, "A symmetrical condensed node for the TLM method," *IEEE Trans. Microwave Theory Tech.*, vol. 35, pp. 370–377, 1987.
[9] P. Naylor and R. A. Desai, "New three dimensional symmetrical condensed lossy node for solution of electromagnetic wave problems by TLM," *Electron. Lett.*, vol. 26, pp. 492–494, 1990.
[10] D. H. Staelin, A. W. Morgenthaler, and J. A. Kong, *Electromagnetic Waves.* Englewood Cliffs, NJ: Prentice-Hall, 1994.
[11] A. Ishimaru, *Electromagnetic Wave Propagation, Radiation, and Scattering.* Englewood Cliffs, NJ: Prentice-Hall, 1991.
[12] J. A. Morente, G. Gimenez, J. A. Porti, and M. Khalladi, "Dispersion analysis for a TLM mesh of symmetrical condensed nodes with stubs," *IEEE Trans. Microwave Theory Tech.*, vol. 43, pp. 452–456, 1995.

Ian G. Gosling (SM'93) was born in Hitchin, U.K., in 1955. He received the B.A. degree in natural sciences (physics) in 1977, and the M.A. and Ph.D. degrees in microwave engineering in 1981, all from the University of Cambridge, U.K.

In 1981, he joined British Telecom Research Laboratories, working on millimeter-wave integrated circuits, monolithic circuits and test systems, and computer-aided design. In 1988, he was appointed a Senior Lecturer for the School of Electrical and Electronic Engineering, Nanyang Technological University, Singapore. He has published some 20 papers and holds several patents. His current research interests include computer-aided modeling of microwave components and communications systems.

Pingyu Qu was born in Chengdu, Sichuan, China, in 1969. He received the B.Eng. degree in microwave engineering in 1990 from the University of Electronic Science and Technology of China (UESTC), China, From 1993 to 1994, he worked toward the M.S. degree at the Institute of Applied Physics, UESTC, China. Currently, he is an M.Eng. student in the School of Electrical and Electronic Engineering, Nanyang Technological University, Singapore.

From 1990 to 1993, he worked as an Assistant Engineer in the area of high-power microwave technology for the Institute of Applied Electronics, Chinese Academy of Engineering Physics, P.R.C. His current research interest is in TLM simulation of electromagnetic problems.